frontiers in Energy Research

ORIGINAL RESEARCH
published: 24 January 2022
doi: 10.3389/fenrg.2021.795513

A Dynamic and Cooperative Control Strategy for Multi-Hybrid Energy Storage System of DC Microgrid Based on SOC

Hao Li, Lijun Fu, Yan Zhang and Yiyong Xiong*

National Key Laboratory of Science and Technology on Vessel Integrated Power System, Naval University of Engineering, Wuhan, China

With the increasingly serious crisis of fossil energy and environmental pollution, clean renewable energy becomes the inevitable choice of energy structure adjustment. The instability of output power of distributed renewable energy system greatly affects the operation of DC microgrid. The hybrid energy storage system (HESS) composed of High-Energy Battery (HEB) and High-Power Battery (HPB) can solve the above problems. Thus, this paper proposes a dynamic and cooperative control strategy for multi-HESS based on state of charge (SOC). Based on the traditional LPF method and droop control, this paper proposes a control strategy that requires no communication among multiple hybrid energy storage (HES) modules. This method can realize the stable control of HEB current, reduce the change times of HEB charging-discharging mode, prevent HEB from overcharging and overdischarging, prolong the service life of HEB and balance different energy storage SOC, so as to improve the operation stability and economy of DC microgrid. In addition, the method has certain robustness against sudden failures. Simulation and experiment results show the effectiveness of the proposed method.

Keywords: DC microgrid, distributed access, multi-hybrid energy storage system (multi-HESS), dynamic balance of SOC, renewable energy

OPEN ACCESS

Edited by:
Haoran Zhao,
Shandong University, China

Reviewed by:
Yuji Zeng,
Dalian Maritime University, China
Bo Wang,
University of New South Wales, Australia
Salman Hajiaghasi,
Shahid Beheshti University, Iran

****Correspondence:***
Hao Li
18351930189@163.com

Specialty section:
This article was submitted to Process and Energy Systems Engineering, a section of the journal Frontiers in Energy Research

Received: *15 October 2021*
Accepted: *20 December 2021*
Published: *24 January 2022*

Citation:
Li H, Fu L, Zhang Y and Xiong Y (2022) A Dynamic and Cooperative Control Strategy for Multi-Hybrid Energy Storage System of DC Microgrid Based on SOC. Front. Energy Res. 9:795513. doi: 10.3389/fenrg.2021.795513

INTRODUCTION

The increasing penetration rate of renewable energy such as photovoltaic and wind power promotes the development of DC microgrid (Kathiresan et al., 2020; Zhou et al., 2020). Compared with AC microgrid, DC microgrid has no problems such as synchronization, reactive power transmission, harmonic current and converter loss, so it has attracted more and more attention (Rahimi and Ghadiriyan, 2019; Song et al., 2019).

However, due to the intermittent impact of renewable energy distributed generation and the short-term impact of some large loads, the stability of DC microgrid is severely challenged. Therefore, the corresponding energy storage system should be equipped to enhance the anti-interference ability of DC microgrid (Singh and Lather, 2021). On the one hand, combining High-Energy Battery (Such as lithium battery, lead-acid battery, sodium sulfur battery) with High-Power Battery (Such as supercapacitor, flywheel energy storage, super-magnetic energy storage) to form HESS is an important way of energy storage configuration based on the existing energy storage technology and satisfying the demand for DC microgrid (Kotra and Mishra, 2019; Mathews and Rajeev, 2020). On the other hand, in order to improve the access flexibility of energy storage system,

and avoid the cost increase of using large-capacity converters in centralized energy storage system and the problems of operational reliability, distributed multi-HESS should be used (Su et al., 2018).

In terms of applying HESS to suppress grid-connected power fluctuations of distributed power generation, many scholars have studied various control strategies according to the characteristics of different types of energy storage, such as LPF method (Manandhar et al., 2015), fuzzy logic control (FLC) (Musilek et al., 2017; Mathews and Rajeev, 2020), wavelet decomposition method (Chiang et al., 2017), layered drooping control (Li et al., 2016; Zhang et al., 2018), virtual inertial control (Ming et al., 2017; Wang et al., 2017), machine learning (Chen et al., 2020) and so on. The above method mainly focuses on centralized HESS, when extended to distributed multi-HESS, they have some inapplicability. With the increase of using time, the differences among HES modules become larger and larger. If not restrained and controlled, the performance of HES modules will be seriously affected.

The concept of a virtual power rating was introduced in Literature (Hoang and Lee, 2019) to achieve accurate power sharing between batteries. However, this control method requires communication, and the scope of its application has certain limitations. In literature (Zhou et al., 2018), multi-HEB SOC is divided into five regions, and the whole system is divided into six working modes. However, this method may switch modes frequently under the circumstance of high-frequency fluctuation, leading to system instability. Most importantly, the above literatures mainly focus on the cooperative control of multiple energy storage units with the same medium and the same property.

In view of the collaborative control problem of distributed multi-HESS in DC microgrid, a power control strategy for multi-HESS was proposed based on the consensus protocol in literature (Chen et al., 2019). The communication was established among different energy storage units, and the SOC of different energy storage units was balanced by the consensus protocol, thus effectively solving the problem of balanced power distribution among multi-HESS. In literature (Wu et al., 2020), the control system automatically switches the operating mode based on the DC bus voltage, the supercapacitor voltage and the accumulator state. However, these methods still depend on external communication and are not suitable for situations requiring high reliability. To solve this problem, literature (Chen et al., 2016) proposed voltage-current droop control for HEB and voltage-change rate-current droop control for HPB. When the system only relies on the local information of the energy storage, it realizes the automatic power distribution between the components of different types of energy storage. However, this method is controlled by difference, and the deviation of bus voltage is large.

In order to solve the problem of high dependence on external communication in power distribution, this paper takes the island operation of DC microgrid as the research object, based on the traditional LPF method and droop control, proposes a SOC based power secondary distribution method without communication among HES modules. The control system automatically redistributes power according to SOC of different energy storage to achieve SOC balance. The smooth control of HEB current can be realized by using the characteristic that HPB voltage cannot change suddenly, so as to reduce the number of charging-discharging mode changes of HEB and extend the service life of HEB. The effectiveness of the proposed control strategy for distributed multi-hybrid energy storage module parallel system is verified by simulation and experiment.

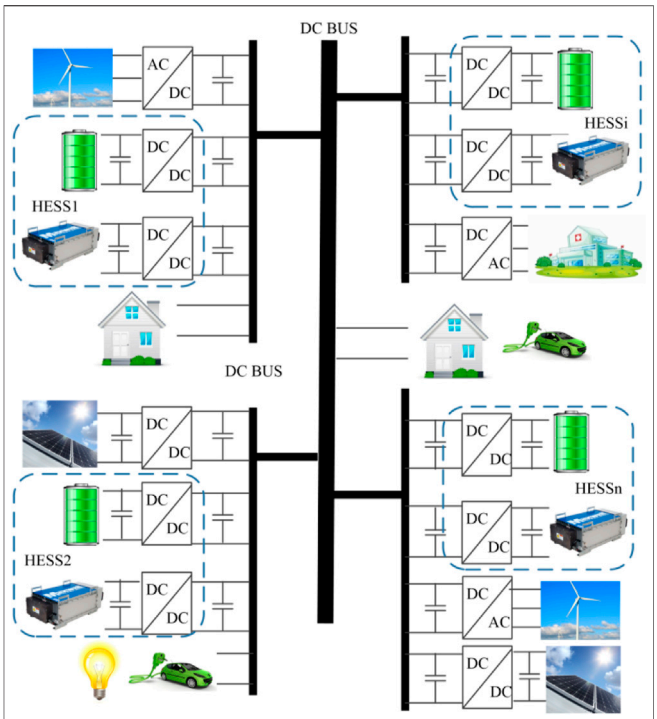

FIGURE 1 | Schematic diagram of DC microgrid with multi-HESS.

SYSTEM MODEL

The schematic diagram of DC microgrid with multi-HESS is shown in **Figure 1**, which mainly includes renewable energy power generation unit, AC/DC load and energy storage unit. Each part is a distributed structure, and each unit is connected to the DC bus through the corresponding converter. The power relationship of each part is as follows:

$$P_{\mathrm{Gen}} + P_{\mathrm{HESS}} = P_{\mathrm{Load}} \tag{1}$$

P_{Gen} is the power generated by renewable energy, P_{HESS} is the total power of multi-HESS, and P_{Load} is the total load power, including AC load and DC load.

In system analysis and calculation, the load of renewable energy power generation and power electronic equipment access can be equivalent to a controllable current source, which can be positive or negative. When it is positive, the renewable energy power generation is greater than the load; when negative, the load is greater than the renewable energy power generation.

HESS in **Figure 1** consists of High-Energy Battery and High-Power Battery. High-Energy Battery has high energy density and

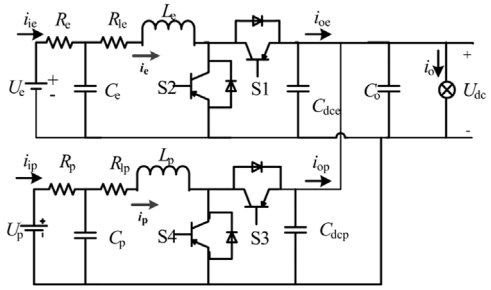

FIGURE 2 | Single HES module topology.

long storage time, but low power density and low cycle times. High-Power Battery has high power density and high cycle times, but low energy density and short energy storage time.

The single HES module topology adopted in this paper is shown in **Figure 2**. U_e and U_p, R_e and R_p are the voltage and resistance of High-Energy Battery and High-Power Battery respectively. U_{dc} is the DC bus voltage. The converter in the **Figure 2** is a bidirectional Buck-Boost converter. C_e and C_p, L_e and L_p are respectively the filter capacitance and inductance of the converters. R_{le} and R_{lp} are the internal resistance of respective inductors. S1-S4 are power tubes. C_{dce} and C_{dcp} are filter capacitors of converters respectively. C_o is the bus voltage regulator capacitor. (Subscript "e" means High-Energy Battery, and subscript "p" means High-Power Battery.)

COOPERATIVE CONTROL STRATEGY FOR MULTI-HESS

The overall architecture of multi-HESS collaborative control strategy is shown in **Figure 3**. The improved LPF control structure is adopted to regulate the power distribution within the single HES module. Based on the HPB SOC, the output power of HEB and HPB inside the module is adjusted to maintain the HPB SOC in a healthy range as far as possible. Among the multiple HES modules, the output of the whole module is regulated through the reference bus voltage adaptive regulator based on HEB SOC, so as to maintain the overall available capacity of each HES module relatively consistent. Since each HES module adopts V-I droop control, the coordinated control among HES modules does not require communication, which has high reliability and scalability, plug and play, and is convenient for installation and deployment.

Basic Control Structure

In microgrid, there are many control methods for converters, among which droop control is a widely used decentralized control method. It does not need communication, and only uses local information to realize the coordination control between distributed power supplies. It is suitable for DC microgrid with high reliability requirements, such as islands, reefs and ships, etc. Therefore, in order to maximize the autonomous control of each HES module, and enhance the system reliability and "plug and play" capability, the converter of HESS adopts droop control to stabilize the DC bus voltage.

V-I droop control (Li et al., 2016; Zhang et al., 2018) can be expressed as:

$$U_{o*} = U_{ref} - R_V i_o \tag{2}$$

U_{ref} is the value of DC bus voltage under no load, U_{o*} is the specified value of converter output voltage after correction, and R_V is the droop coefficient.

The value of R_V is determined by **Eq. 3**:

$$R_V = (U_{ref} - U_{omin})/I_{omax} \tag{3}$$

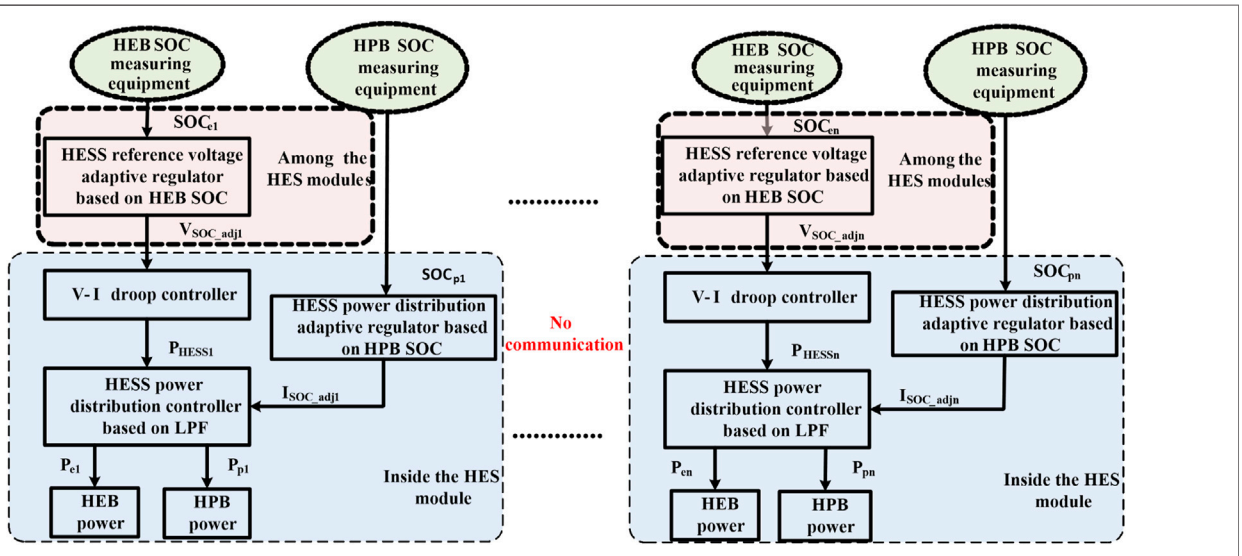

FIGURE 3 | The overall architecture of multi-HESS collaborative control strategy.

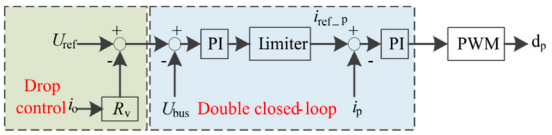

FIGURE 4 | The control structure diagram of High-Power Battery.

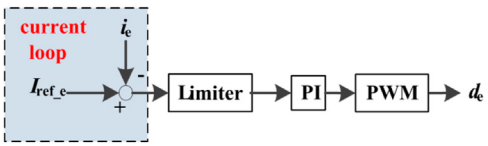

FIGURE 5 | The control structure diagram of High-Energy Battery.

U_{omin} is the allowable minimum steady state value of DC bus voltage, and I_{omax} is the maximum current value that DC/DC converter can output/input.

Ignoring the line impedance, the output current relationship of several DC/DC converters with V-I droop control is shown as follows.

$$R_{V1}i_{o1} = \ldots = R_{Vk}i_{ok} = \ldots = R_{Vn}i_{on} \tag{4}$$

The control structure of High-Power Battery consists of a droop control outer loop and a voltage and current double closed-loop, as shown in **Figure 4**. U_{ref}, U_{bus} and I_{ref_p} respectively represent the reference voltage of the bus, the actual voltage of the bus and the reference current of the High-Power Battery.

HEB is mainly used to follow the current instructions given by the power distribution controller, as shown in **Figure 5**. I_{ref_e} and i_e respectively represent the reference current and the actual current of the High-Energy Battery.

HES Module Control Based on LPF

Figure 6 is the control structure diagram of LPF-based. Reasonable power distribution method is the key to the stability and reliability of HESS. The traditional LPF method has less computation and parameters, and the control is simple. It can realize the power distribution based on frequency without any communication. Thus, this paper adopts LPF method for power distribution. On the basis of the traditional LPF control, the adaptive power redistribution module is added to regulate the output of different energy storage units in real time and balance the remaining electric quantity. The adaptive power redistribution modules represented by the two blue squares are described in detail in the next section.

iDC_{HESSi} is the sum of the current at the bus end of the DC/DC converter in the ith HES module, as shown in **Eq. 5**. i_{ei} and i_{pi} are the current of High-Energy Battery and High-Power Battery in the ith HES module, while d_{ei} and d_{pi} are the control signals of DC/DC converter. The limiter prevents the reference current from exceeding the converter maximum current.

$$iDC_{HESSi} = iDC_{ei} + iDC_{pi} \tag{5}$$

iDC_{ei} and iDC_{pi} are the current at the bus end of the DC/DC converter connected with High-Energy Battery and the High-Power Battery in the ith HES module.

Overall Idea of Adaptive SOC Layered Control

During the use of the HESS, there are different initial SOC and rated capacity of each energy storage unit connected by the converter in a certain working condition. If SOC are not considered, some energy storage units may overcharge or overdischarge, affecting the stable operation of the whole system. Therefore, the balanced control of energy storage SOC is the key to the stable and economical operation of HESS.

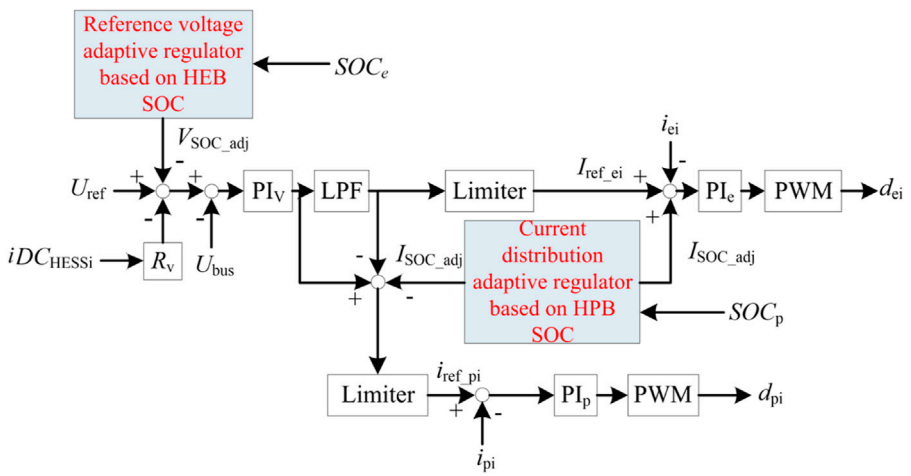

FIGURE 6 | The control structure diagram of LPF-based.

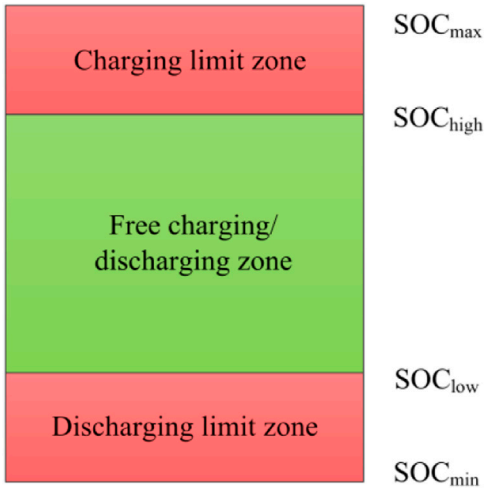

FIGURE 7 | SOC restriction classification of energy storage unit.

In order to prevent energy storage units from overcharging/overdischarging and frequent charging/discharging change, this paper adopts adaptive SOC layered control strategy. According to the SOC level of each energy storage unit, it is divided into different operating range as shown in **Figure 7**.

(1) Free charging/discharging zone. When $SOC_{low} \leq SOC \leq SOC_{high}$, the energy storage unit can conduct normal charge/discharge in accordance with the droop relationship, without imposing other control operations based on SOC.
(2) Charging limit zone. When $SOC_{high} \leq SOC \leq SOC_{max}$, the energy storage charging will be limited, and as SOC gets closer and closer to SOC_{max}, the charging limit becomes more and more serious until no more charging is allowed.
(3) Discharging limit one. When $SOC_{min} \leq SOC \leq SOC_{low}$, the energy storage discharging will be limited, and as SOC gets closer and closer to SOC_{min}, the discharging limit becomes more and more serious until no more discharging is allowed.

Adaptive SOC Control Method Inside the HES Module

In HESS, power fluctuation is usually divided into low frequency and high frequency, which are borne by High-Energy Battery and High-Power Battery respectively. The response speed of High-Power Battery is obviously faster than that of High-Energy Battery. DC microgrid is operating in island mode, the High-Power Battery will quickly compensate the power shortage in case of sudden change of load. When the High-Power Battery responds quickly, its SOC fluctuates. Then, the High-Energy Battery responds slowly to maintain the stability of the High-Power Battery SOC, achieving a dynamic adaptive balance. Through such a master-slave double structured with adaptive control, the system will gradually transfer the power deficiency firstly borne by the High-Power Battery to the High-Energy Battery, which can make the High-Energy Battery charge/discharge change relatively smooth, reduce the depth of the charge/discharge, prolong the life of High-Energy Battery, and avoid overcharge/overdischarge of High-Power Battery.

The ampere-hour integral method is used to calculate the SOC of High-Power Battery (Manandhar et al., 2015).

$$SOC_p = SOC_{p0} - \frac{1}{C_{Np}} \int_0^T \mu_p i_p \partial t \tag{6}$$

SOC_p is the real-time SOC of High-Power Battery, SOC_{p0} is the initial SOC, T is the running time, μ_p is the charging/discharging efficiency, i_p is the charging/discharging current, C_{Np} is the rated capacity of the HPB.

According to the layered control principle introduced in **Figure 5**, partial charging/discharging current of High-Power Battery is transferred to the High-Energy Battery. This paper designs I_{SOC_adj} that is the current of the High-Power Battery transferred to the High-Energy Battery based on the concept of partition operation as shown in **Figure 7**. The specific expression is shown in **Eq. 7**:

$$I_{SOC\_adj} = \begin{cases} \dfrac{SOC_p - SOC_{plow}}{SOC_{p\,min} - SOC_{plow}} I_{ref\_p} \left(SOC_{p\,min} \leq SOC_p \leq SOC_{plow}, V_{diff} > 0\right) \\ \dfrac{SOC_p - SOC_{phigh}}{SOC_{p\,max} - SOC_{phigh}} I_{ref\_p} \left(SOC_{phigh} \leq SOC_p \leq SOC_{p\,max}, V_{diff} < 0\right) \\ 0 \qquad \text{(othor)} \end{cases} \tag{7}$$

I_{ref_P} refers to the initial reference current of the High-Power Battery, and V_{diff} refers to the difference between the reference voltage and the actual voltage of the bus, which is used to characterize the charging and discharging state of energy storage unit at this time.

$$V_{diff} = U_{ref} - U_{bus} \tag{8}$$

$V_{diff} > 0$ means the energy storage unit is in charge, and $V_{diff} < 0$ means it is in discharge.

$$I_{ref\_p*} = I_{ref\_p} - I_{SOC\_adj} \tag{9}$$

$$I_{ref\_e*} = I_{ref\_e} + I_{SOC\_adj} \tag{10}$$

$I_{ref\_p^*}$ and $I_{ref\_e^*}$ represent the regulated High-Power Battery and High-Energy Battery reference current.

According to **Eqs 7–10**, when the High-Power Battery is in the charging limit zone, a certain proportion of the charging current is transferred to the High-Energy Battery according to the current SOC_p. The higher the SOC_p is, the larger the proportion of the transferred current will be. On the contrary, when the High-Power Battery is in the discharging limit zone, situation is the opposite. Finally, the High-Power Battery SOC is always in a reasonable operating range.

Among the HES Modules

High-Power Battery has low energy density. The adaptive regulating frequency of power among HES modules is much lower than that in a single HES module, so the High-Energy

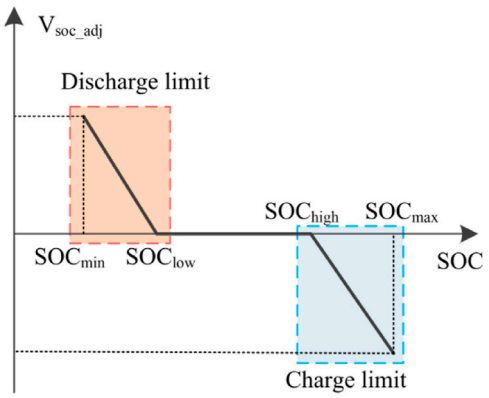

FIGURE 8 | Piecewise linearization regulation model based on SOC.

Battery SOC can be used as an indicator of the whole HES module available capacity.

The ampere-hour integral method is used to calculate the SOC of High-Energy Battery (Manandhar et al., 2015).

$$SOC_e = SOC_{e0} - \frac{1}{C_{Ne}} \int_0^T \mu_e i_e \partial t \tag{11}$$

SOC_e is the real-time SOC of High-Energy Battery, SOC_{e0} is the initial SOC, T is the running time, μ_e is the charging/discharging efficiency, i_e is the charging/discharging current, C_{Ne} is the rated capacity of the HEB.

The proposed adaptive regulation strategy of reference voltage based on SOC is used to regulate the reference voltage of droop control model.

$$U_{bus} = U_{ref} - V_{SOC\_adj} - R_V i_o \tag{12}$$

V_{SOC_adj} is the reference voltage regulation. In order to improve the regulation performance of the strategy and avoid system oscillation caused by re-regulation of critical SOC, the layered regulation framework shown in **Figure 7** is adopted. The specific algorithm is as follows:

$$V_{SOC\_adj} = \begin{cases} k\dfrac{SOC_e - SOC_{elow}}{SOC_{e\min} - SOC_{elow}} & (SOC_{e\min} \le SOC_e \le SOC_{elow}, V_{diff} > 0) \\ k\dfrac{SOC_{ehigh} - SOC_e}{SOC_{e\max} - SOC_{ehigh}} & (SOC_{ehigh} \le SOC_e \le SOC_{e\max}, V_{diff} < 0) \\ 0 & (othor) \end{cases} \tag{13}$$

k is the proportional amplification gain, which is determined by the maximum power of the converter and the requirement of the system on the regulation ability.

According to **Eqs 12**, **13** when the SOC of an energy storage unit is in the charging limit zone, the reference voltage value of the DC/DC convert output should be increased to reduce the charging current of the energy storage unit. On the contrary, when the SOC is in the discharging limit zone, the situation is the opposite. Finally, SOC of different energy storage units tends to be relatively consistent. The specific process is shown in **Figure 8**, where the X-axis is the SOC of energy storage unit and the Y-axis is the regulator of the reference voltage value of the DC/DC convert output. The model is simple and easy to implement, and the switching between modes is relatively smooth.

STABILITY ANALYSIS AND CONTROL PARAMETER SELECTION

Stability Analysis Model

Because the control strategy proposed in this paper presents a coupling state inside a single HES module, it is difficult to adopt impedance analysis method. Thus, this paper intends to adopt small-signal analysis method to establish a mathematical analysis model for a single HES module as a whole.

Since resistive load increases system damping, constant power load (CPL) decreases system damping. So in the worst case, assume that the load on the system contains only CPL. Once the system is stable in the worst case, it is stable in all cases. Thus, in the study, the load will select the CPL, which can be expressed as:

$$i_{Load} = \frac{P_{CPL}}{u_{dc}} \tag{14}$$

i_{Load} is load current, P_{CPL} is load power, u_{dc} is bus voltage transient value.

The small signal model can be obtained as follows:

$$\Delta i_{Load} = \frac{P_{CPL}}{U_{dc}^2} \Delta u_{dc} \tag{15}$$

U_{dc} is steady-state value of bus voltage at equilibrium point.

The state equation of the main circuit is shown in **Eq. 16**:

$$\begin{cases} L_p \dfrac{di_p}{dt} = u_p - R_p i_p - (1 - d_p) u_{dc} \\ L_e \dfrac{di_e}{dt} = u_e - R_e i_e - (1 - d_e) u_{dc} \\ C_{dc} \dfrac{du_{dc}}{dt} = (1 - d_p) i_p + (1 - d_e) i_e - \dfrac{P_{CPL}}{u_{dc}} \end{cases} \tag{16}$$

d_e and d_p are the duty cycle instantaneous value of HEB and HPB control signal.

The small signal model can be obtained as follows:

$$\begin{cases} L_p \Delta \hat{i_p} = -R_p \Delta i_p - (1 - D_p) \Delta u_{dc} + U_{dc} \Delta d_p \\ L_e \Delta \hat{i_e} = -R_e \Delta i_e - (1 - D_e) \Delta u_{dc} + U_{dc} \Delta d_e \\ C_{dc} \Delta \widehat{u_{dc}} = (1 - D_p) \Delta i_p - I_p \Delta d_p + (1 - D_e) \Delta i_e - I_e \Delta d_e - \dfrac{P_{CPL}}{U_{dc}^2} \Delta u_{dc} \end{cases} \tag{17}$$

Eq. 17 is written in matrix form:

$$\Delta \hat{x_1} = \mathbf{A}_1 \Delta x_1 + \mathbf{B}_1 \Delta u_1 \tag{18}$$

$$\Delta x_1 = \begin{bmatrix} \Delta i_p & \Delta i_e & \Delta u_{dc} \end{bmatrix}^T \quad \Delta u_1 = \begin{bmatrix} \Delta d_e & \Delta d_p \end{bmatrix}^T$$

$$\mathbf{A}_1 = \begin{bmatrix} -\frac{R_p}{L_p} & 0 & \frac{D_p - 1}{L_p} \\ 0 & -\frac{R_e}{L_e} & \frac{D_e - 1}{L_e} \\ \frac{1 - D_p}{C_{dc}} & \frac{1 - D_e}{C_{dc}} & \frac{P_{CPL}}{C_{dc}U_{dc}^2} \end{bmatrix} \quad \mathbf{B}_1 = \begin{bmatrix} 0 & \frac{U_{dc}}{L_p} \\ \frac{U_{dc}}{L_e} & 0 \\ \frac{-I_e}{C_{dc}} & \frac{-I_p}{C_{dc}} \end{bmatrix}$$

The small-signal model of the HEB control loop in **Figure 6**:

$$\hat{X}_v = U_{ref} - R_v\left[(1 - d_e)i_e + (1 - d_p)i_p\right] - u_{dc} - V_{SOC\_adj} \quad (19)$$

$$I_{DCref} = k_{vi}X_v + k_{vp}\hat{X}_v \quad (20)$$

$$I_{ref\_e} = \frac{1}{1 + T_f s}I_{DCref} \quad (21)$$

$$\hat{X}_{ie} = \left(I_{ref\_e} + \frac{U_p}{U_{dc}}I_{SOC\_adj}\right)\frac{U_{dc}}{U_e} - i_e \quad (22)$$

X_v and X_{ie} are the steady-state values of the input of the voltage loop and the current loop in the control loop of HEB. I_{DCref} is the total current reference value, I_{ref_e} is the current reference value of HEB, T_f is the filtering time constant of the low-pass filter, k_{vp} and k_{vi}, k_{ep} and k_{ei} are the PI parameters of the voltage loop and the current loop in the control loop of HEB.

The deformation of **Eq. 21** can be obtained as follows:

$$\hat{I_{ref\_e}} = \frac{1}{T_f}I_{DCref} - \frac{1}{T_f}I_{ref\_e} \quad (23)$$

The duty cycle of HEB converter can be expressed as:

$$d_e = k_{ei}X_{ie} + k_{ep}\hat{X}_{ie} \quad (24)$$

The control loop of HPB can be expressed as:

$$I_{ref\_p} = I_{DCref} - I_{ref\_e} \quad (25)$$

$$\hat{X}_{ip} = \frac{U_{dc}}{U_p}I_{ref\_p} - i_p - I_{SOC\_adj} \quad (26)$$

X_{ip} is the steady-state input value of the current loop in the HPB control loop, I_{ref_p} is the current reference value of the HPB, and k_{pp} and k_{pi} are the PI parameters of the current loop in the HPB control loop.

$$d_p = k_{pi}X_{ip} + k_{pp}\hat{X}_{ip} \quad (27)$$

In combination with **Eqs 24**, **27**, the small-signal model can be written as:

$$\Delta u_1 = \mathbf{B}_{11}\Delta x_1 + \mathbf{B}_{12}\Delta x_2 + \mathbf{B}_{13}\Delta x_3 + \mathbf{B}_2\Delta u_1 \quad (28)$$

$$\Delta x_2 = \begin{bmatrix} \Delta X_v & \Delta X_{ie} & \Delta X_{ip} & \Delta I_{ref\_e} \end{bmatrix}^T$$

$$\Delta x_3 = \begin{bmatrix} \Delta V_{SOC\_adj} & \Delta I_{SOC\_adj} \end{bmatrix}^T$$

$$\mathbf{B}_{11} = \begin{bmatrix} 0 & -k_{ep} & 0 \\ -k_{pp}k_{vp}R_v\frac{U_{dc}}{U_p}(1 - D_p) - k_{pp} & -k_{pp}k_{vp}R_v\frac{U_{dc}}{U_p}(1 - D_e) & -k_{pp}k_{vp}\frac{U_{dc}}{U_p} \end{bmatrix}$$

$$\mathbf{B}_{12} = \begin{bmatrix} 0 & k_{ei} & 0 & k_{ep}\frac{U_{dc}}{U_e} \\ k_{pp}k_{vi}\frac{U_{dc}}{U_p} & 0 & k_{pi} & -k_{pp}\frac{U_{dc}}{U_p} \end{bmatrix}$$

$$\mathbf{B}_{13} = \begin{bmatrix} 0 & k_{ep}\frac{U_{dc}}{U_e} \\ -k_{pp}k_{vp}\frac{U_{dc}}{U_p} & -k_{pp} \end{bmatrix}$$

$$\mathbf{B}_2 = \begin{bmatrix} 0 & 0 \\ k_{pp}k_{vp}R_vI_e\frac{U_{dc}}{U_p} & k_{pp}k_{vp}R_vI_p\frac{U_{dc}}{U_p} \end{bmatrix}$$

The state vector Δx_2 of the controller variable can be expressed as:

$$\Delta\hat{x_2} = \mathbf{A}_{21}\Delta x_1 + \mathbf{A}_{22}\Delta x_2 + \mathbf{A}_{23}\Delta x_3 + \mathbf{B}_3\Delta u_1 \quad (29)$$

According to **Eqs 12–22** and **25**, **26**, we can get:

$$\mathbf{A}_{21} = \begin{bmatrix} -R_v(1 - D_p) & -R_v(1 - D_e) & -1 \\ 0 & -1 & 0 \\ -k_{vp}R_v(1 - D_p)\frac{U_{dc}}{U_p} - 1 & -k_{vp}R_v(1 - D_e)\frac{U_{dc}}{U_p} & -k_{vp}\frac{U_{dc}}{U_p} \\ \frac{-k_{vp}R_v(1 - D_p)}{T_f} & \frac{-k_{vp}R_v(1 - D_e)}{T_f} & \frac{-k_{vp}}{T_f} \end{bmatrix}$$

$$\mathbf{A}_{22} = \begin{bmatrix} 0 & 0 & 0 & 0 \\ 0 & 0 & 0 & \frac{U_{dc}}{U_e} \\ k_{vi}\frac{U_{dc}}{U_p} & 0 & 0 & -\frac{U_{dc}}{U_p} \\ \frac{k_{vi}}{T_f} & 0 & 0 & \frac{-1}{T_f} \end{bmatrix} \mathbf{A}_{23} = \begin{bmatrix} -1 & 0 \\ 0 & \frac{U_p}{U_e} \\ -k_{vp}\frac{U_{dc}}{U_p} & -1 \\ -\frac{k_{vp}}{T_f} & 0 \end{bmatrix}$$

$$\mathbf{B}_3 = \begin{bmatrix} R_vI_e & R_vI_p \\ 0 & 0 \\ k_{vp}R_vI_e\frac{U_{dc}}{U_p} & k_{vp}R_vI_p\frac{U_{dc}}{U_p} \\ \frac{k_{vp}R_vI_e}{T_f} & \frac{k_{vp}R_vI_p}{T_f} \end{bmatrix}$$

The upper control input vector Δx_3 can be expressed as:

$$\Delta\hat{x}_3 = \mathbf{A}_{31}\Delta x_1 + \mathbf{A}_{32}\Delta x_2 + \mathbf{A}_{33}\Delta x_3 + \mathbf{B}_4\Delta u_1 \quad (30)$$

The energy storage unit has an integral relation between SOC and time. Despite the existence of such an integral relationship, the present state value of the SOC is calculated and output by sampling, so the changes of the output current and voltage are difficult to reflect the changes of the SOC in very short time. Therefore, the SOC is only treated as an input signal in small signal modeling. At the same time, considering that the change of SOC is not as rapid

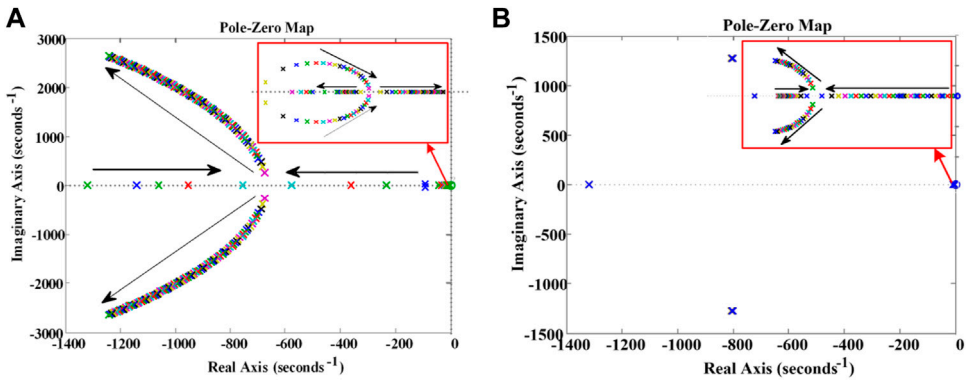

FIGURE 9 | Closed-loop pole distribution of voltage outer loop PI parameters: **(A)** The scale parameter k_{vp} increases from 0.1 to 20; **(B)** The integral parameter k_{vi} increases from 0.1 to 50).

TABLE 1 | The simulation parameters.

Parameters	Value
Bus voltage rating/V	400
Energy storage terminal filter capacitance C_e, C_p/μF	20
Bus terminal filter capacitance C_{dce}, C_{dcp}, C_o/μF	940
Filter inductance L_e, L_p/H	0.001
Filter inductance internal resistance R_e, R_p, R_{le}, R_{lp}/Ω	0.01
Bus voltage regulator capacity C_e, C_p/μF	4000
Filtering time constant/T_f	1
NO.1,2,3 High-Energy Battery rated capacity/Ah	15, 13, 12
NO.1,2,3 High-Power Battery rated capacity/Ah	5, 5, 4

TABLE 2 | PI parameter.

Parameter name	Value	Parameter name	Value
k_{vp}	5	k_{vi}	35
k_{ep}	0.003	k_{ei}	0.4
k_{pp}	0.003	k_{pi}	1

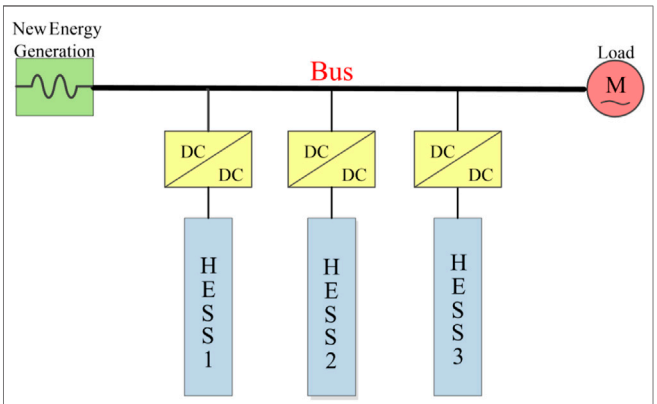

FIGURE 10 | The overall simulation model.

as the change of voltage and current, delay sampling strategy is generally adopted, and LPF can be used to replace short delay.

As V_{SOC_adj} and I_{SOC_adj} are both piecewise functions in the optimization of upper power allocation considering SOC. In the stability analysis, only the case with the worst stability is considered, that is, they are all in the discharge limit region:

$$V_{SOC\_adj} = \frac{w}{w+s} k \frac{SOC_e - SOC_{elow}}{SOC_{e\,min} - SOC_{elow}} \left(SOC_{e\,min} \le SOC_e \le SOC_{elow}, V_{diff} > 0\right) \tag{31}$$

$$I_{SOC\_adj} = \frac{w}{w+s} \frac{SOC_p - SOC_{plow}}{SOC_{p\,min} - SOC_{plow}} I_{pref} \left(SOC_{p\,min} \le SOC_p \le SOC_{plow}, V_{diff} > 0\right) \tag{32}$$

Small signal transformation is performed for **Eqs 31**, **32**:

$$\Delta \hat{V}_{SOC\_adj} = -w\Delta V_{SOC\_adj} \left(SOC_{e\,min} \le SOC_e \le SOC_{elow}, V_{diff} > 0\right) \tag{33}$$

$$\Delta \hat{I}_{SOC\_adj} = \begin{cases} w \dfrac{SOC_p - SOC_{plow}}{SOC_{p\,min} - SOC_{plow}} \Delta I_{pref} - w\Delta I_{SOC\_adj} \\ \left(SOC_{p\,min} \le SOC_p \le SOC_{plow}, V_{diff} > 0\right) \end{cases} \tag{34}$$

w is the cutoff frequency of LPF.

In summary, the following formula can be obtained by combining **Eqs 19**, **20** and **25**:

$$\mathbf{A}_{31} = \begin{bmatrix} 0 & 0 & 0 \\ -wMk_{vp}R_v(1-D_p) & -wMk_{vp}R_v(1-D_e) & -wMk_{vp} \end{bmatrix}$$

$$\mathbf{A}_{32} = \begin{bmatrix} 0 & 0 & 0 & 0 \\ wMk_{vi} & 0 & 0 & -wM \end{bmatrix} \quad \mathbf{A}_{33} = \begin{bmatrix} -w & 0 \\ -wMk_{vp} & -w \end{bmatrix}$$

$$\mathbf{B}_4 = \begin{bmatrix} 0 & 0 \\ wMk_{\mathrm{vp}}R_{\mathrm{v}}I_{\mathrm{e}} & wMk_{\mathrm{vp}}R_{\mathrm{v}}I_{\mathrm{p}} \end{bmatrix} \quad M = \frac{SOC_{\mathrm{p}} - SOC_{\mathrm{plow}}}{SOC_{\mathrm{p\,min}} - SOC_{\mathrm{plow}}}$$

By comprehensively considering **Eqs 18**, **29**, **30**, it can be obtained:

$$\begin{bmatrix} \Delta\dot{x}_1 . \\ \Delta\dot{x}_2 . \\ \Delta\dot{x}_3 . \end{bmatrix} = \begin{bmatrix} \mathbf{X}_{11} & \mathbf{X}_{12} & \mathbf{X}_{13} \\ \mathbf{X}_{21} & \mathbf{X}_{22} & \mathbf{X}_{23} \\ \mathbf{X}_{31} & \mathbf{X}_{32} & \mathbf{X}_{33} \end{bmatrix} \times \begin{bmatrix} \Delta x_1 \\ \Delta x_2 \\ \Delta x_3 \end{bmatrix} \begin{cases} \mathbf{X}_{11} = \mathbf{A}_1 + \mathbf{B}_1 (1 - \mathbf{B}_2)^{-1} \mathbf{B}_{11} \\ \mathbf{X}_{12} = \mathbf{B}_1 (1 - \mathbf{B}_2)^{-1} \mathbf{B}_{12} \\ \mathbf{X}_{13} = \mathbf{B}_1 (1 - \mathbf{B}_2)^{-1} \mathbf{B}_{13} \\ \mathbf{X}_{21} = \mathbf{A}_{21} + \mathbf{B}_3 (1 - \mathbf{B}_2)^{-1} \mathbf{B}_{11} \\ \mathbf{X}_{22} = \mathbf{A}_{22} + \mathbf{B}_3 (1 - \mathbf{B}_2)^{-1} \mathbf{B}_{12} \\ \mathbf{X}_{23} = \mathbf{A}_{23} + \mathbf{B}_3 (1 - \mathbf{B}_2)^{-1} \mathbf{B}_{13} \\ \mathbf{X}_{31} = \mathbf{A}_{31} + \mathbf{B}_4 (1 - \mathbf{B}_2)^{-1} \mathbf{B}_{11} \\ \mathbf{X}_{32} = \mathbf{A}_{32} + \mathbf{B}_4 (1 - \mathbf{B}_2)^{-1} \mathbf{B}_{12} \\ \mathbf{X}_{33} = \mathbf{A}_{33} + \mathbf{B}_4 (1 - \mathbf{B}_2)^{-1} \mathbf{B}_{13} \end{cases} \quad (35)$$

Stability Analysis and Control Parameter Selection

Figure 9 is the closed-loop pole distribution diagram of **Eq. 35** when different PI parameters are selected (the black arrow indicates the increasing direction of the parameters taken). SOC limited boundaries of High-Energy Batteries and High-Power Batteries SOC_{min}, SOC_{max}, SOC_{low}, SOC_{high} respectively are 50, 70, 56, 63, and 40, 80, 55, 65%. Other specific simulation parameters are shown in **Table 1**.

It can be seen from **Figure 9** that when k_{vi} and k_{vp} change in the specified range, the system pole is always on the left of the Y-axis, so the system is always stable. As shown in **Figure 9A**, the poles close to the imaginary axis are conjugate poles when the voltage outer loop proportionality parameter k_{vp} is less than 6, and it is an underdamped system. At the same time, with the increase of k_{vp}, the damping ratio of the system gradually increases, and the overshoot decreases. Therefore, when k_{vp} = 5, the overshoot of the system is small and the response speed is fast. As shown in **Figure 9B**, when k_{vi} is greater than 30, the closed loop dominates the pole conjugate. At this time, the system has good dynamic response characteristics. As k_{vi} continues to increase, the peak value of the system decreases, but the response time increases. Therefore, the trade-off is k_{vi} = 35.

The same method is adopted for other control parameters and their stability analysis. The PI parameters of the proposed method are obtained and summarized as shown in **Table 2**.

SIMULATION AND EXPERIMENT

In this paper, PSCAD/EMTDC software will be used for simulation. In order to fully verify the performance of the proposed HESS control strategy, three groups of HESS will be set up. HESS1 is overdischarged, HESS2 is in the free charging/discharging zone, and HESS3 is overcharged. The structure of each group is shown in **Figure 2**. The overall simulation model is shown in **Figure 10**. In this simulation, lithium battery is used for HEB and supercapacitor is used for HPB. Simulation parameters are shown in **Tables 1**, **2**.

Step Load Change

In this case, the response of the system to consecutive step load changes is simulated to observe the net power decomposition between High-Energy Battery and High-Power Battery. The specific waveform is shown in **Figure 11A**. At 10 s, the load current increases from 50 to 125 A, then drops back to 50 A at 25 s, and finally jumps to 150 A at 50 s. The initial SOC of three High-Energy Batteries and High-Power Batteries are 55, 62, 67, 60, 70%. To verify the effectiveness of the proposed strategy, it will be compared with the LPF-based HESS control method without SOC regulation, that is, the control method shown in **Figure 5** removes the SOC regulation module represented by the blue square. The results are shown in **Figures 11B–K**.

It can be seen from **Figures 11B,C** that both methods can effectively cope with the step change of load and make the deviation of bus voltage stable within 2.5%. However, the voltage deviation rate of the proposed method is reduced by about 50%.

Figures 11D–G shows that SOC of each energy storage unit cannot be balanced without SOC regulation. Considering the practical differences of energy storage units, SOC difference will become larger and larger, eventually leading to the overcharge or overdischarge of some energy storage units. However, under the SOC coordinated control method proposed in this paper, SOC can tend to be consistent which can effectively prevent some energy storage units from overcharging/overdischarging, and improve the stability and reliability of the system.

According to the comparison among **Figures 11H–K**, it can be seen that under the SOC regulation, the energy storage unit with SOC higher than the limit increases its output power when discharging. The energy storage unit with SOC lower than the limit decreases output power when discharging. Under this regulation, SOC of each energy storage unit will gradually tend to be consistent. At the same time, High-Power Battery quickly responds to sudden load change, then gradually falls back, and gradually transfers the power shortage to the High-Energy Battery. In other words, frequency distribution is realized in the HESS, and the output/input current of the High-Energy Battery is smoothed, which effectively extends the service life of the High-Energy Battery and improves the economy and reliability of the energy storage system.

Random Fluctuations in Renewable Energy Generation

Considering the random fluctuation of renewable energy, the response characteristics of High-Energy Battery and High-Power Battery in the control strategy proposed in this paper are studied. The initial state of each energy storage unit is consistent with the previous section. **Figure 12** shows the output curve of renewable energy adopted in simulation, the power response and SOC changing of High-Energy Batteries and High-Power Batteries.

From **Figures 12B,C**, it can be seen that multi-HESS can effectively make real-time power compensation in the case of

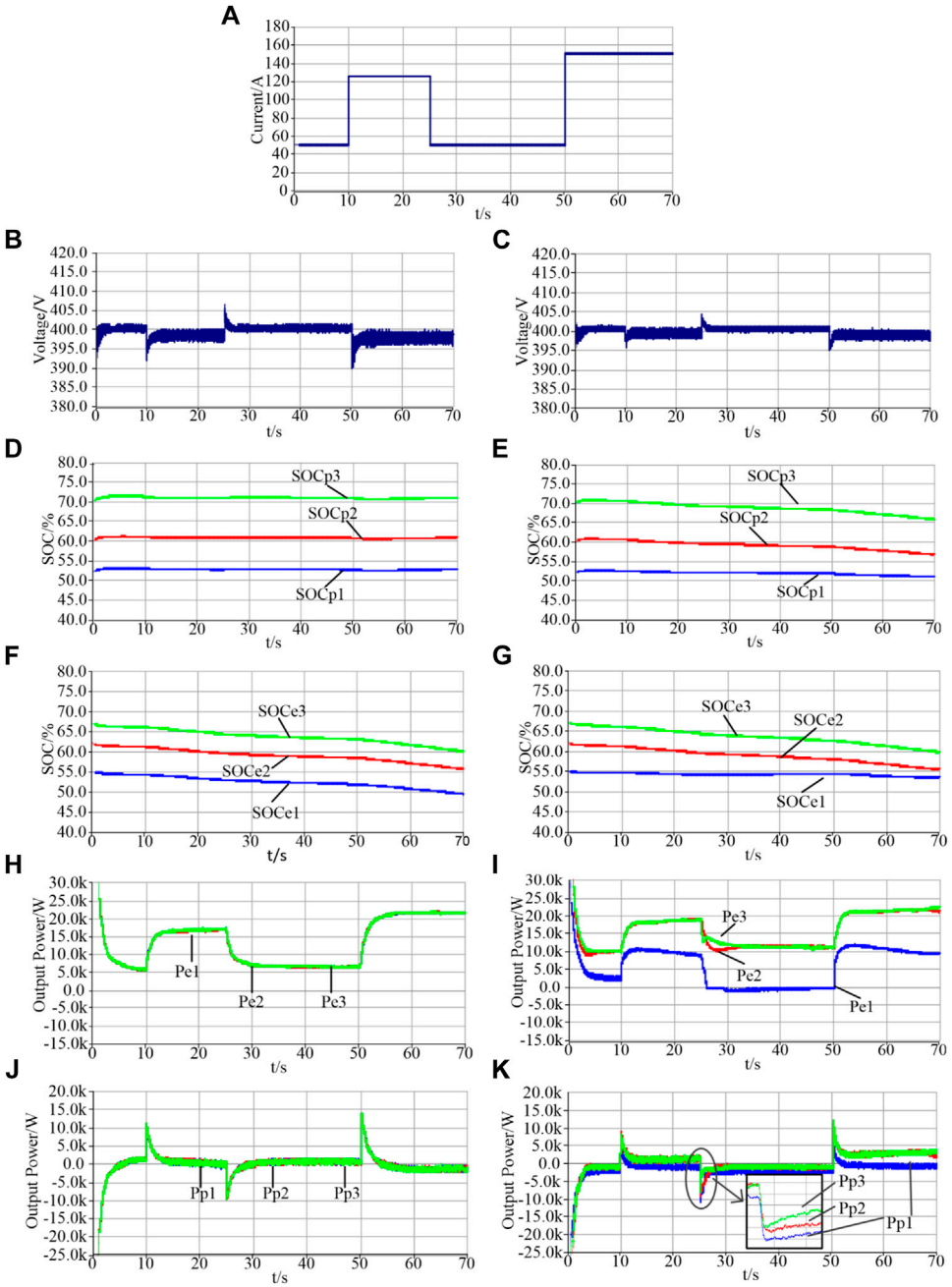

FIGURE 11 | Simulation results under step load condition: **(A)** Load current; **(B)** Bus voltage-No SOC regulation; **(C)** Bus voltage-SOC regulation; **(D)** High-Power Battery SOC-No SOC regulation; **(E)** High-Power Battery SOC-SOC regulation; **(F)** High-Energy Battery SOC-No SOC regulation; **(G)** High-Energy Battery SOC-SOC regulation; **(H)** The output power of High-Energy Battery-No SOC regulation; **(I)** The output power of High-Energy Battery-SOC regulation; **(J)** The output power of High-Power Battery-No SOC regulation; **(K)** The output power of High-Power Battery-SOC regulation).

random fluctuation of renewable energy. The partial power compensated by the High-Energy Batteries is more gradual than that of the High-Power Batteries and achieves the expected frequency distribution effect.

At the same time, from **Figures 12D,E**, the output of different High-Energy Battery and High-Power Battery varies due to SOC differences and the energy storage output power with high SOC is larger, so that SOC tends to be consistent. Moreover, due to the setting of free charging/discharging zone, the regulation of energy storage unit is smoother, reducing the number of charging/discharging mode changes, and effectively extending the service life of energy storage unit. Simulation results show that the proposed control strategy can ensure the

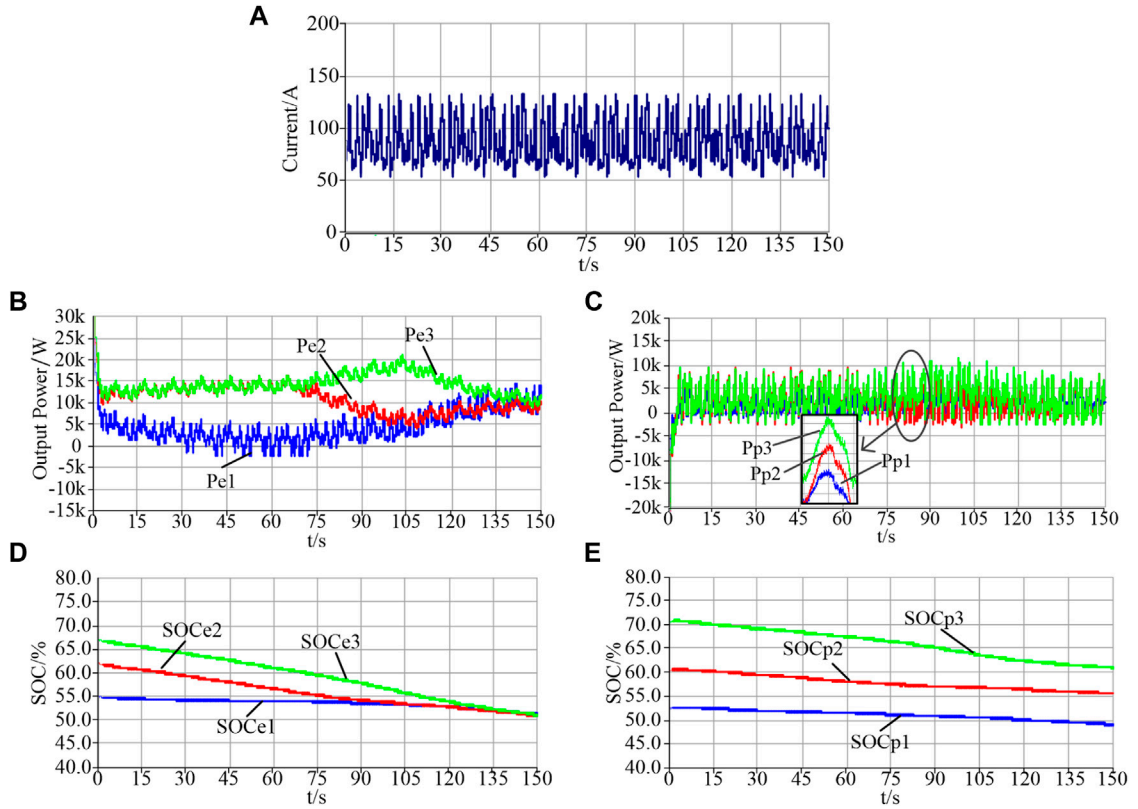

FIGURE 12 | Simulation results under random load condition: **(A)** Random power of renewable energy-Random output of renewable energy; **(B)** Output power of High-Energy Battery; **(C)** Output power of High-Power Battery; **(D)** High-Energy Battery SOC; **(E)** High-Power Battery SOC).

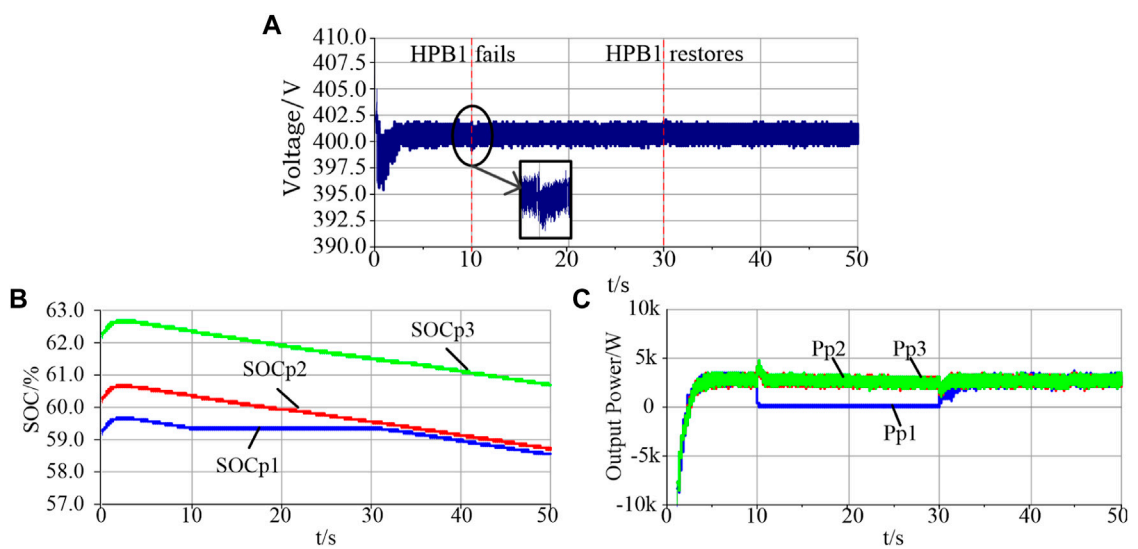

FIGURE 13 | Simulation results when No. 1 High-Power Battery fault: **(A)** Bus voltage; **(B)** High-Power Battery SOC; **(C)** Output power of High-Power Battery).

reasonable operation of the multi-HESS when the random fluctuations of renewable energy are taken into account.

Failure of a High-Power Battery

It is assumed that a High-Power Battery breaks down and runs out, and all energy storage units are in free charging/discharging

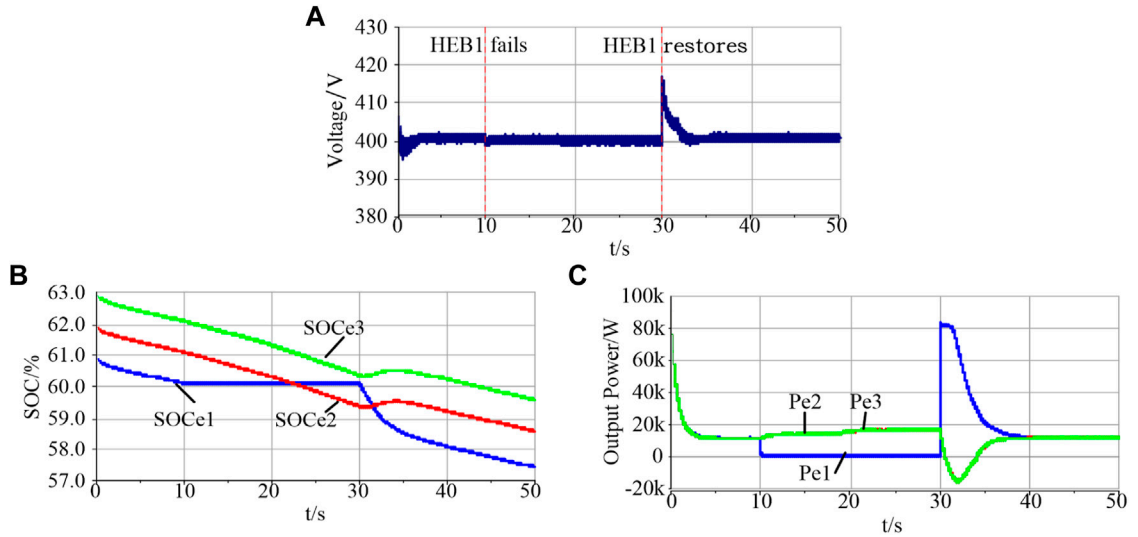

FIGURE 14 | Simulation results when No. 1 High-Energy Battery fault: **(A)** Bus voltage; **(B)** High-Energy Battery SOC; **(C)** Output power of High-Energy Battery).

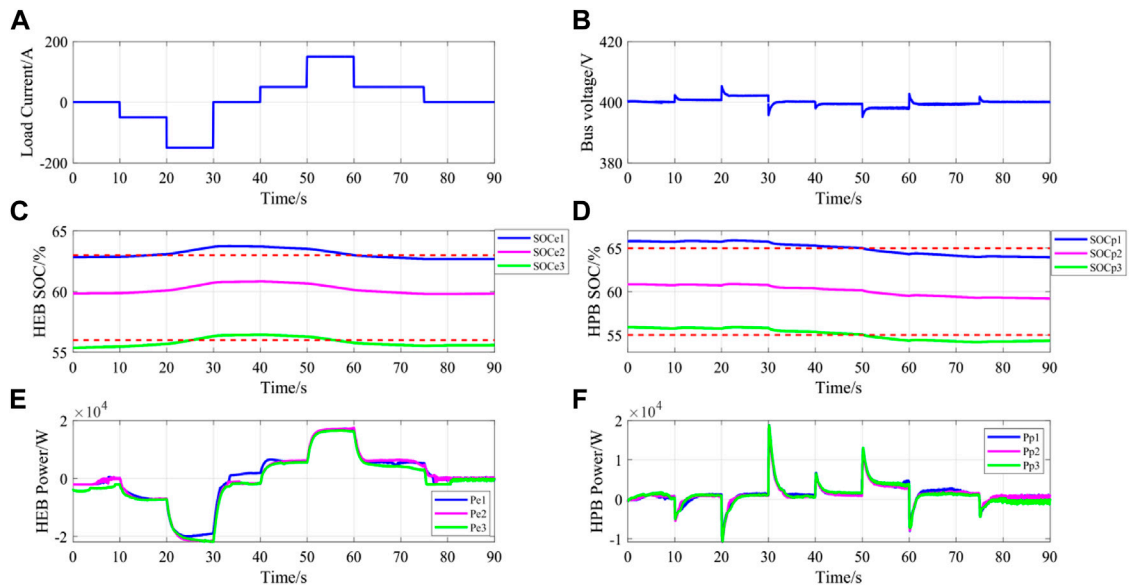

FIGURE 15 | Experimental results of DC microgrid in step load change: **(A)** Load current; **(B)** Bus voltage; **(C)** High-Energy Battery SOC; **(D)** High-Power Battery SOC; **(E)** Output power of High-Energy Battery; **(F)** Output power of High-Power Battery).

zone, so as to verify the stability of the proposed control strategy. Under normal operating conditions, the system is connected to 100 A load. At 10 s, No. 1 High-Power Battery fails, exits operation, and cuts off relevant communication. At 30 s, No. 1 High-Power Battery resumes and puts into operation. The simulation results are shown in **Figure 13**.

Figure 13A shows that when it comes to 10 and 30 s, the cut and input of No. 1 High-Power Battery only causes a small impact on the bus voltage. **Figure 13B** shows that SOC of No. 1 High-Power Battery remains unchanged after failure, while the decline rate of other High-Power Battery increases. After the No. 1 High-Power Battery is repaired and put into operation in 30 s, the SOC of the three groups of High-Power Battery is still in the free charging/discharging zone, so it quickly keeps in sync. It can be seen from **Figure 13C** that the other two groups of High-Power Battery respond quickly at the moment of the cut and input of No. 1 High-Power Battery. Simulation results show that the remaining energy storage under the proposed control strategy can still work normally and respond to the expected power when some High-Power Batteries fail.

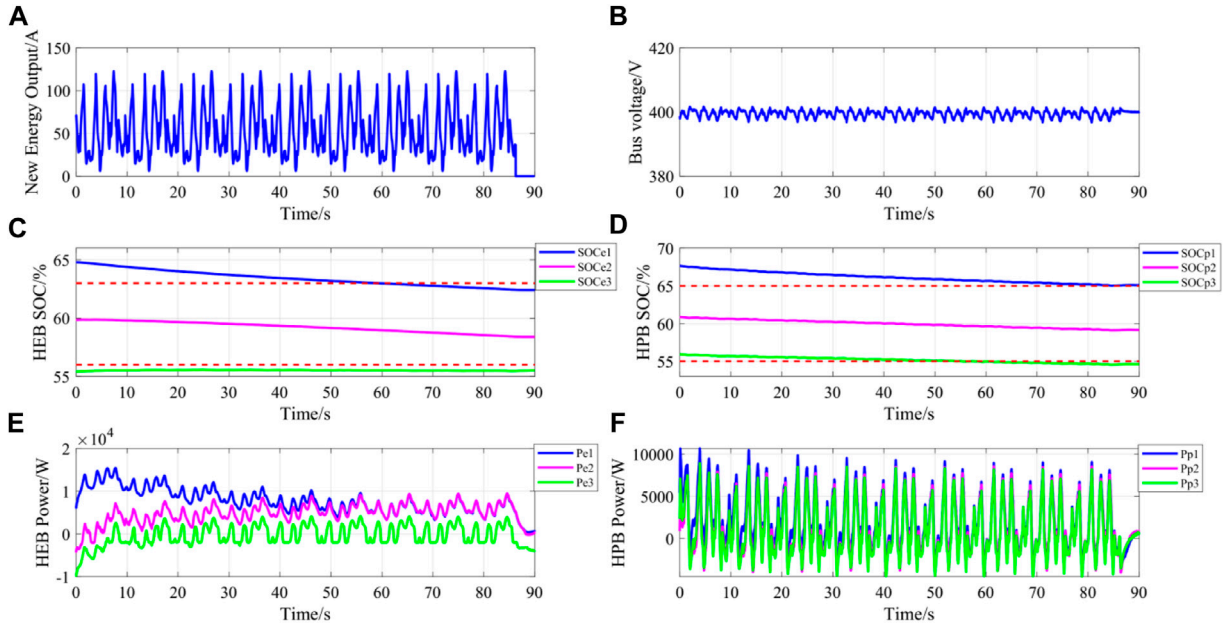

FIGURE 16 | Experimental results of DC microgrid in renewable energy generation: **(A)** Renewable energy output; **(B)** Bus voltage; **(C)** High-Energy Battery SOC; **(D)** High-Power Battery SOC; **(E)** Output power of High-Energy Battery; **(F)** Output power of High-Power Battery).

Failure of a High-Energy Battery

Under the same condition of **section 4.2**, replace the fault unit with No. 1 High-Energy Battery. The simulation results are shown in **Figure 14**.

The results in **Figure 14** are similar to **Figure 13**, but more volatile. The main reason is that the High-Energy Battery has to bear more power in normal operation, and the impact on the system during cutting and input is also greater. But bus voltage deviation is still within a reasonable range, it's not more than 5% and soon returns to the normal reference voltage. The proposed method is robust to partial energy storage element faults.

Experimental Verification and Result Analysis

A microgrid model was established in the laboratory for verification. The analog diesel generator cabinet and analog wind generator cabinet are used as the power supply, the switching frequency of the energy storage bidirectional DC/DC converter is 10 kHz, the load is a programmable DC load, HEB is lithium iron phosphate battery, HPB is supercapacitor and other control parameters are the same as the simulation model. The experimental results are shown in **Figures 15**, **16**.

It can be seen from **Figures 15**, **16A** and **Figures 15**, **16B** that after power fluctuation, the bus voltage can be quickly restored to stability with small voltage fluctuation. **Figures 15**, **16E** and **Figures 15**, **16F** show the output power changes of HEB and HPB. As can be seen from the figure, the change of HEB is relatively slow, while the response of HPB to power fluctuation is fast, which is in line with the design goal of the control strategy. Combined with the SOC change curves in **Figures 15**, **16C** and **Figures 15**, **16D**, it can be seen that the power curve of energy storage when SOC is higher than the limited range moves upward, that is, the discharge power is higher while the charge power is lower. When SOC is below the limit range, the power curve of energy storage moves downward, that is, the discharge power is lower while the charge power is higher. This shows that the proposed control strategy can effectively carry out SOC balancing.

CONCLUSION

Aiming at the problem that the traditional distributed multi-HESS cooperative control method of DC microgrid relies heavily on external communication, a communication free dynamic cooperative control strategy based on SOC is proposed. The simulation and experiment results show that the proposed control strategy has the following advantages: *1*) being able to adjust the power distribution within HES module and among HES modules meet the needs of large-scale distributed new energy generating sets and loads; *2*) using HPB to respond to the high frequency component of the bus voltage fluctuation, and using HEB to compensate the insufficient power of HPB to realize the optimization of HEB charge-discharge current, so as to effectively reduce the number of HEB charge-discharge mode change and prolong its service life; *3*) reducing the dependency on communication among HES modules, thus improving the

reliability of DC microgrid in island mode. However, this method does not take into account the impact of energy storage element aging, such as SOC estimation errors and reduced maximum output power due to declining energy storage life. How to consider these aspects under the condition of minimal communication requirements will be the focus of future research.

DATA AVAILABILITY STATEMENT

The raw data supporting the conclusions of this article will be made available by the authors, without undue reservation.

AUTHOR CONTRIBUTIONS

HL completed the theoretical derivation, modeling and simulation, data analysis and full text drafting of the project. YZ and YX provided research direction, theoretical guidance and paper revision. LF provided theoretical guidance, financial and site support.

FUNDING

This work was supported by the National Natural Science Foundation of China under Grant 51877211.

REFERENCES

Chen, H., Zhang, Z., Guan, C., and Gao, H. (2020). Optimization of Sizing and Frequency Control in Battery/supercapacitor Hybrid Energy Storage System for Fuel Cell Ship. *Energy* 197, 117285. doi:10.1016/j.energy.2020.117285

Chen, M., Zhao, X., Jin, X., Liu, J., and Wu, X. (2016). Research on Parallel Technology of Compound Energy Storage Device in DC Microgrid [J]. *Trans. China Electrotechnical Soc.* 31 (a02), 142–149. doi:10.19595/j.cnki.1000-6753.tces.2016.s2.016

Chen, X., Shi, M., Zhou, J., Chen, Y., Zuo, W., and Wen, J. (2019). Distributed Cooperative Control of Multiple Hybrid Energy Storage Systems in a DC Microgrid Using Consensus Protocol[J]. *IEEE Trans. Ind. Electro.*, 1968–1979. doi:10.1109/TIE.2019.2898606

Chiang, P. H., Chiluvuri, S. P. V., Dey, S., and Nguyen, T. Q. (2017). "Forecasting of Solar Photovoltaic System Power Generation Using Wavelet Decomposition and Bias-Compensated Random Forest[C]," in 2017 Ninth Annual IEEE Green Technologies Conference (GreenTech), Denver, CO, USA, 29–31 March 2017.

Hoang, K. D., and Lee, H.-H. (2019). Accurate Power Sharing with Balanced Battery State of Charge in Distributed DC Microgrid. *IEEE Trans. Ind. Electron.* 66 (3), 1883–1893. doi:10.1109/tie.2018.2838107

Kathiresan, J., Natarajan, S. K., and Jothimani, G. (2020). Energy Management of Distributed Renewable Energy Sources for Residential DC Microgrid Applications [J]. *Int. Trans. Electr. Energ. Syst.* 30 (3), e12258. doi:10.1002/2050-7038.12258

Kotra, S., and Mishra, M. K. (2019). "Design and Stability Analysis of DC Microgrid with Hybrid Energy Storage System[J]. *IEEE Trans. Sustain. Energy* PP (3), 1-1.1603-1612. doi:10.1109/TSTE.2019.2891255

Li, J., Rui, X., Yang, Q., Liang, F., and Zhang, M. (2016). Design/test of a Hybrid Energy Storage System for Primary Frequency Control Using a Dynamic Droop Method in an Isolated Microgrid Power System[J]. *Appl. Energ.* 201, 257. doi:10.1016/j.apenergy.2016.10.066

Manandhar, U., Ukil, A., Kollimalla, S. K., and Gooi, H. B. (2015). "Application of HESS for PV System with Modified Control Strategy[C]," in 2015 7th IEEE Innovative Smart Grid Technologies Conference-ISGT Asia, Bangkok, Thailand, 3–6 Nov. 2015.

Mathews, M. A., and Rajeev, T. (2020). "Fuzzy Based Management of Hybrid Energy Storage System for Improved Dynamic Response of DC Microgrid[C]," in 2020 IEEE International Conference on Power Electronics, Smart Grid and Renewable Energy (PESGRE), Cochin, India, 2–4 Jan. 2020.

Ming, Y. U., Wang, Y., and Li, Y. G. (2017). Virtual Inertia Control of Hybrid Energy Storage in DC Microgrid Based on Predictive Method[J]. *Power Syst. Tech.* 41 (5), 7. doi:10.13335/j.1000-3673.pst.2016.1947

Musilek, P., Krömer, P., Martins, R., and Hesse, H. C. (2017). "Optimal Energy Management of Residential PV/HESS Using Evolutionary Fuzzy Control[C]," in 2017 IEEE Congress on Evolutionary Computation (CEC), Donostia, Spain, 5–8 June 2017.

Rahimi, M., and Ghadiriyan, S. (2019). A Generalized Droop-Based Compensator for Addressing the Issues Raised in a DC Microgrid Comprising Hybrid Wind-Battery-Back up Generation Sources[J]. *Int. Trans. Electr. Energ. Syst.* 29 (9), e12052. doi:10.1002/2050-7038.12052

Singh, P., and Lather, J. S. (2021). Power Management and Control of a Grid-independent DC Microgrid with Hybrid Energy Storage System. *Sustainable Energ. Tech. Assessments* 43, 100924. doi:10.1016/j.seta.2020.100924

Song, W., Chen, Y., Zhang, Y., Wen, A., and Wei, C. (2019). Bidirectional Boost Converter for High-power Transmission Between Energy Storage Battery and DC Microgrid. *Electron. Lett.* 55 (7), 402–404. doi:10.1049/el.2018.7561

Su, H., Zhang, J., Wang, N., and Guo, W. (2018). Energy Management Strategy of High Capacity Hybrid Energy Storage System Based on Hierarchical Optimization[J]. *High-Voltage Tech.* 44 (4), 1177–1186. doi:10.7500/AEPS20160729015

Wang, Y., Hei, Y., Fu, Y., Wu, Z. K., and Yang, P. H. (2017). Adaptive Virtual Inertia Control of Dc Distribution Network Based on Variable Droop Coefficient[J]. *Automation Electric Power Syst.* 41 (8), 116–124. doi:10.19595/j.cnki.1000-6753.tces.171119

Wu, T., Ye, F., Su, Y., Wang, Y., and Riffat, S. (2020). Coordinated Control Strategy of DC Microgrid with Hybrid Energy Storage System to Smooth Power Output Fluctuation. *Int. J. Low-Carbon Tech.* 15 (1), 46–54. doi:10.1093/ijlct/ctz056

Zhang, J. H., Wang, H. M., Wei, Y. L., et al. (2018). The Layered Control Strategy of Dc Micro-grid Bus Voltage Fluctuation Including Composite Energy Storage and Gas Turbine Generator[J]. *Trans. China Electrotechnical Soc.* 33 (6), 1238–1246.

Zhou, G., Tian, Q., Leng, M., Fan, X., and Bi, Q. (2020). Energy Management and Control Strategy for DC Microgrid Based on DMPPT Technique. *IET Power Electro.* 13 (4), 658–668. doi:10.1049/iet-pel.2019.0383

Zhou, J. P., Zhang, W. Z., Wang, T., Li, X. Y., Li, X. Q,, and Mao, D. J. (2018). Multi-cell Control Strategy Based on Power Interaction and Dynamic Distribution[J]. *High-Voltage Tech.* 44 (4), 1149–1156. doi:10.13336/j.1003-6520.hve.20180329014

Conflict of Interest: The authors declare that the research was conducted in the absence of any commercial or financial relationships that could be construed as a potential conflict of interest.

Publisher's Note: All claims expressed in this article are solely those of the authors and do not necessarily represent those of their affiliated organizations, or those of the publisher, the editors and the reviewers. Any product that may be evaluated in this article, or claim that may be made by its manufacturer, is not guaranteed or endorsed by the publisher.